nanomaterials

MDPI

Article

Cobalt Ferrite Nanorods Synthesized with a Facile "Green" Method in a Magnetic Field

Alexander L. Kwiatkowski [1,*], Petr V. Shvets [2], Ivan S. Timchenko [1], Darya E. Kessel [1], Elizaveta D. Shipkova [1], Konstantin I. Maslakov [3], Ivan A. Kuznetsov [1], Dmitry A. Muravlev [1], Olga E. Philippova [1] and Andrey V. Shibaev [1,4,*]

1 Physics Department, Lomonosov Moscow State University, Leninskije Gory 1-2, 119991 Moscow, Russia; ivan.s.timchenko@gmail.com (I.S.T.); dkshmr@yandex.ru (D.E.K.); shipkova_liza@mail.ru (E.D.S.); pusido0907@yandex.ru (I.A.K.); mit89-angel@yandex.ru (D.A.M.); phil@polly.phys.msu.ru (O.E.P.)
2 REC "Functional Nanomaterials", Immanuel Kant Baltic Federal University, Aleksandra Nevskogo St., 14, 236041 Kaliningrad, Russia; pshvets@kantiana.ru
3 Chemistry Department, Lomonosov Moscow State University, Leninskije Gory 1-3, 119991 Moscow, Russia; nonvitas@gmail.com
4 Chemistry Department, Karaganda E.A. Buketov University, University Street 28, Karaganda 100028, Kazakhstan
* Correspondence: kvyatkovskij@physics.msu.ru (A.L.K.); shibaev@polly.phys.msu.ru (A.V.S.)

Abstract: We report a new facile method for the synthesis of prolate cobalt ferrite nanoparticles without additional stabilizers, which involves a co-precipitation reaction of Fe^{3+} and Co^{2+} ions in a static magnetic field. The magnetic field is demonstrated to be a key factor for the 1D growth of cobalt ferrite nanocrystals in the synthesis. Transmission electron microscopy (TEM), X-ray diffraction (XRD), and Raman spectroscopy are applied to characterize the morphology and structure of the obtained nanoparticles. According to TEM, they represent nanorods with a mean length of 25 nm and a diameter of 3.4 nm that have a monocrystalline structure with characteristic plane spacing of 2.9 Å. XRD and Raman spectroscopy confirm the spinel $CoFe_2O_4$ structure of the nanorods. After aging, the synthesized nanorods exhibit maximum saturation magnetization and coercivity equal to 30 emu/g and 0.3 kOe, respectively. Thus, the suggested method is a simple and "green" way to prepare $CoFe_2O_4$ nanorods with high aspect ratios and pronounced magnetic properties, which are important for various practical applications, including biomedicine, energy storage, and the preparation of anisotropic magnetic nanocomposites.

Keywords: anisotropy; cobalt ferrite; co-precipitation; crystal growth; magnetic field; nanorods

Citation: Kwiatkowski, A.L.; Shvets, P.V.; Timchenko, I.S.; Kessel, D.E.; Shipkova, E.D.; Maslakov, K.I.; Kuznetsov, I.A.; Muravlev, D.A.; Philippova, O.E.; Shibaev, A.V. Cobalt Ferrite Nanorods Synthesized with a Facile "Green" Method in a Magnetic Field. *Nanomaterials* **2024**, *14*, 541. https://doi.org/10.3390/nano14060541

Academic Editors: Paolo M. Scrimin, Sandrine Gerber-Lemaire and Yannick Mugnier

Received: 22 February 2024
Revised: 14 March 2024
Accepted: 18 March 2024
Published: 20 March 2024

1. Introduction

In recent years, high attention has been attracted to the synthesis and investigation of magnetic nanomaterials [1–3], which can be used in many areas, such as the preparation of magnetic nanocomposites and gels [4,5], soft robotics [6], energy storage devices [7], green energy production [8], and various biomedical applications [9,10], including hyperthermia [11], magnetic resonance imaging [12], the development of magnetically responsive industrial systems [13], and so forth. For such nanomaterials, anisotropic (cylindrical, plate-like, etc.) magnetic nanoparticles (NPs) are of high interest [14–16] because of their enhanced magnetic properties [17], anisotropy of magnetism, a larger area of the locally induced magnetic field in comparison to nanospheres, etc. [10], as well as their ability to impart anisotropy to nanocomposite materials.

Various methods for synthesis of elongated magnetic NPs have been described, including solvothermal [18], hydrothermal [19], sol–gel [20] or co-precipitation [21] reactions, ultrasound treatment [22], synthesis in the presence of polymers [23] or surfactants [24–26], modification of the crystal structure of pre-synthesized rod-like particles [12], etc. In most

of these approaches, either a template or a stabilizer is used to provide the growth of NPs in one direction. After synthesis, the surface of NPs usually remains covered with the stabilizer, which may complicate its further modification with organic or inorganic compounds.

Recently, the use of a magnetic field as a template for the 1D growth of magnetic NPs was proposed [27–33]. For instance, a facile and "green" method for the synthesis of elongated magnetite (Fe_3O_4) nanoparticles was elaborated, which consists of the co-precipitation of Fe^{3+} and Fe^{2+} ions in a magnetic field [30,31]. This method allowed obtaining cylindrical Fe_3O_4 NPs of different lengths of up to 150 nm and magnetizations of ca. 29 emu/g. A growth mechanism was proposed, which includes the appearance of small spherical "seed" nanoparticles at the first reaction stage, which then self-assemble into a rod in the external magnetic field and fuse to form a cylindrical NP [32]. The magnetic field was further applied for the synthesis of several 1D nanomaterials, mostly nanowires [33].

Most of the approaches for anisotropic NP synthesis described above are rather well developed for iron oxides, such as magnetite or maghemite. It seems reasonable to apply this method to the preparation of other kinds of magnetic NPs; for instance, cobalt ferrite ($CoFe_2O_4$) NPs, which are of high interest for practical applications due to high coercivity [34] and chemical stability [35]. Current methods of the synthesis of anisotropic cobalt ferrite NPs are rather complex and involve additional compounds [36–38]. For instance, 25 nm × 120 nm $CoFe_2O_4$ nanorods were synthesized by a hydrothermal reaction at 130 °C in the presence of cetyltrimethylammonium bromide [38]. Further studies reported the hydrothermal synthesis of cobalt ferrite nanorods doped with Gd^{3+} ions [39] or Pr^{3+} ions [40] in the absence of surfactants. Micrometer-sized cobalt ferrite rods were obtained by thermal decomposition at 400–700 °C of a $CoFe_2(C_2O_4)_3$ precursor prepared by a solvothermal reaction [41]. There is only one work in which small (several nm) isotropic cobalt ferrite NPs were assembled into rod-like microaggregates during the thermal decomposition of iron(III) and cobalt(II) acetylacetonates in oleic acid, oleylamine, and a benzyl ether at 200 °C under the gradient magnetic field [42]. However, those microaggregates did not represent single crystals but were composed of individual spherical NPs.

In this article, for the first time, we apply the synthesis in a magnetic field to prepare single-crystal cobalt ferrite nanorods. We evidence that a static magnetic field of 0.4 T is sufficient to obtain single-crystal NPs with a length of 25 nm and a diameter of 3.4 nm, which exhibit stronger superparamagnetic properties than the corresponding isotropic NPs. One can expect that such magnetic-field-assisted 1D growth may be further applied to other magnetic metal oxides as well.

2. Materials and Methods

2.1. Materials

Iron(III) chloride hexahydrate ($FeCl_3 \cdot 6H_2O$, purity > 97%) and cobalt(II) nitrate hexahydrate ($Co(NO_3)_2 \cdot 6H_2O$, purity > 98%) were purchased from Sigma-Aldrich (Steinheim, Germany). Sodium hydroxide (purity > 98%, residual water content < 15%) was obtained from Acros (Geel, Belgium). All chemicals were used without further purification. The solutions were prepared in distilled deionized water purified by the Millipore Milli-Q system (Burlington, MA, USA).

2.2. Synthesis of NPs

Synthesis of NPs was performed by a precipitation reaction of Fe^{3+} and Co^{2+} ions in an alkaline solution. The solution of ions with a Fe^{3+}:Co^{2+} molar ratio of 2:1 was prepared by dissolving 2 M $FeCl_3$ and 1 M $Co(NO_3)_2$ in water at magnetic stirring. A total of 2 mL of this solution was put into a reaction vessel kept at 70 °C [43] in the presence or absence of a static magnetic field of 0.4 T created by a permanent NdFeB magnet. Then, 2.5 mL of 6.5 M NaOH was added to the reaction medium, and the reaction was allowed to proceed for 4 h. At the end of the reaction, pH was ca. 6.3, which was measured with a MettlerToledo SevenMulti pH meter(Columbus, OH, USA). To increase the magnetic properties, the solution of NPs was aged at 80 °C. The aging time varied from 1 to 250 h. The final product

was separated from the liquid by magnetic decantation and washed with distilled water. The purification was repeated 3 times.

2.3. Transmission Electron Microscopy

For TEM and high-resolution (HR) TEM measurements, the samples were diluted 10 times with distilled water and after that sonicated for 40 min in pulse mode (5 s of pulses followed by 5 s of rest) with a Sonics VCX 500 ultrasonicator (Newtown, CT, USA) to break the aggregates of NPs. Then, 10 µL of the NP solution was placed onto a 140 mesh Formvar-coated copper grid and air-dried for 3 min at 25 °C. TEM images were obtained using a JEM 2100 F/Cs (Jeol, Tokyo, Japan) operated at 200 kV and equipped with a UHR pole tip as well as a spherical aberration corrector (CEOS, Heidelberg, Germany) and an EEL spectrometer (Gatan, Munich, Germany). The details of the measurements are described elsewhere [44]. The electron micrographs were processed by ImageJ software version 1.54i in order to obtain distances between the crystal planes and to plot the histograms with the NP size distribution [45].

2.4. X-ray Diffraction

The crystal structure of the samples was determined by X-ray diffraction using a Bruker AXS D8 DISCOVER setup with a Cu Kα (wavelength λ = 0.15418 nm) radiation at θ-2θ geometry at room temperature. For measurements, samples were prepared by drying the NP solution on a monocrystalline Si (111) wafer.

2.5. Raman Spectroscopy

The crystal structure and phase composition of the NPs were investigated using a micro-Raman spectrometer LabRam HR800 (Horiba Jobin Yvon, Villeneuve d'Ascq, France) with an ×100 magnification objective (numerical aperture of 0.9). Details of the experimental procedures are described elsewhere [46]. Measurements were conducted at room temperature in the air environment. A He-Ne laser with a 632.8 nm wavelength was used to excite Raman scattering. The irradiation power density on the sample was continuously decreased until no further changes were observed in the spectra obtained. We found that a power of approximately 0.5 mW and a laser spot diameter of about 10 µm were sufficient to avoid structural changes or phase degradation in the films. The spectra were recorded in the range of 100–800 cm^{-1}, and in our measurement conditions, the total acquisition time to obtain a spectrum with a good signal-to-noise ratio was several hours.

2.6. X-ray Photoelectron Spectroscopy

The chemical state of the elements in NPs was analyzed by X-ray photoelectron spectroscopy (XPS) on an Axis Ultra DLD spectrometer (Kratos Analytical, Manchester, UK) with the monochromatic Al Kα X-ray source (1486.7 eV, 150 W) under ultra-high vacuum conditions (10^{-9} mbar). Pass energies of 160 and 40 eV were used, respectively, for survey spectra and high-resolution scans. The powder samples were fixed on a holder using non-conductive double-sided adhesive tape. The Kratos charge neutralizer system was used, and the spectra were charge referenced to give the lattice oxygen component in the O1s spectra a binding energy of 530.1 eV, which is typical for iron oxides [47]. This led to the binding energy of the C1s peak, which is characteristic of adventitious carbon (about 285.0 eV), which confirmed the reliability of the charge reference procedure.

2.7. Magnetometry

The dependencies of magnetization M vs. the applied field strength H of the NPs were measured with a vibrating sample magnetometer, LakeShore 7407 (Westerville, OH, USA) (VSM), at 300 K. The strength of the applied magnetic field varied from −16 to 16 kOe. The samples were dried at room temperature and demagnetized before the measurements. The mean values of saturation magnetization M_s and coercive force H_c were deduced from 3 different measurements.

3. Results and Discussion

In this study, we have synthesized NPs by the co-precipitation of Fe^{3+} and Co^{2+} ions in an alkaline medium. Under a magnetic field of 0.4 T, the elongated rod-like NPs were obtained (Figure 1A). According to TEM data, their mean length <L> and diameter <d_{rod}> are equal to 25 and 3.4 nm, respectively (Figure 2A,B), which corresponds to a rather high aspect ratio of ca. 7. The nanorods co-exist with some spheres indicated by arrows in Figure 1A. The diameter of spheres is ca. 4.7 nm, which is close to that of the nanorods (Figure 2B,C). Previously, the co-existence of spherical NPs with nanorods, grown in the magnetic field, was reported for systems containing magnetite Fe_3O_4 [30,32].

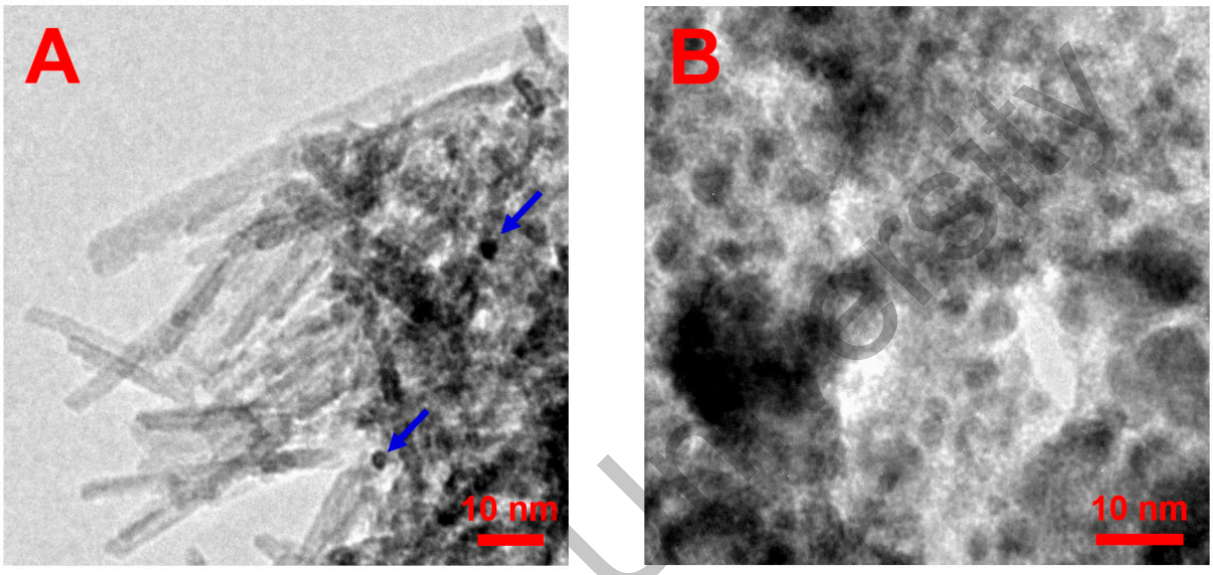

Figure 1. TEM micrographs of NPs synthesized by the co-precipitation of Fe^{3+} and Co^{2+} ions at 70 °C under a magnetic field of 0.4 T (**A**) and in the absence of a magnetic field (**B**). Arrows point out several spheres co-existing with nanorods.

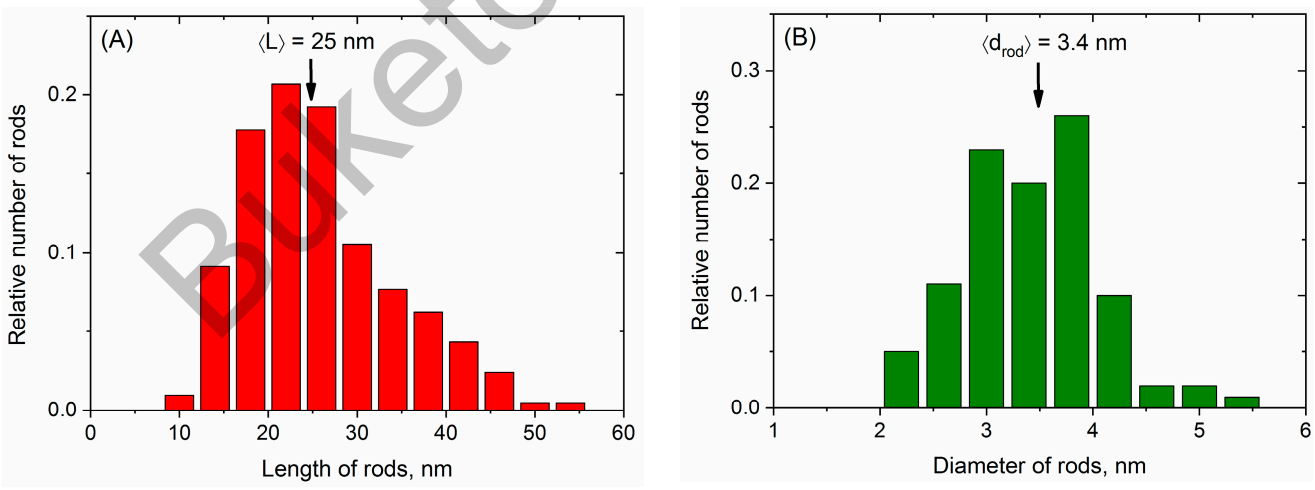

Figure 2. *Cont.*

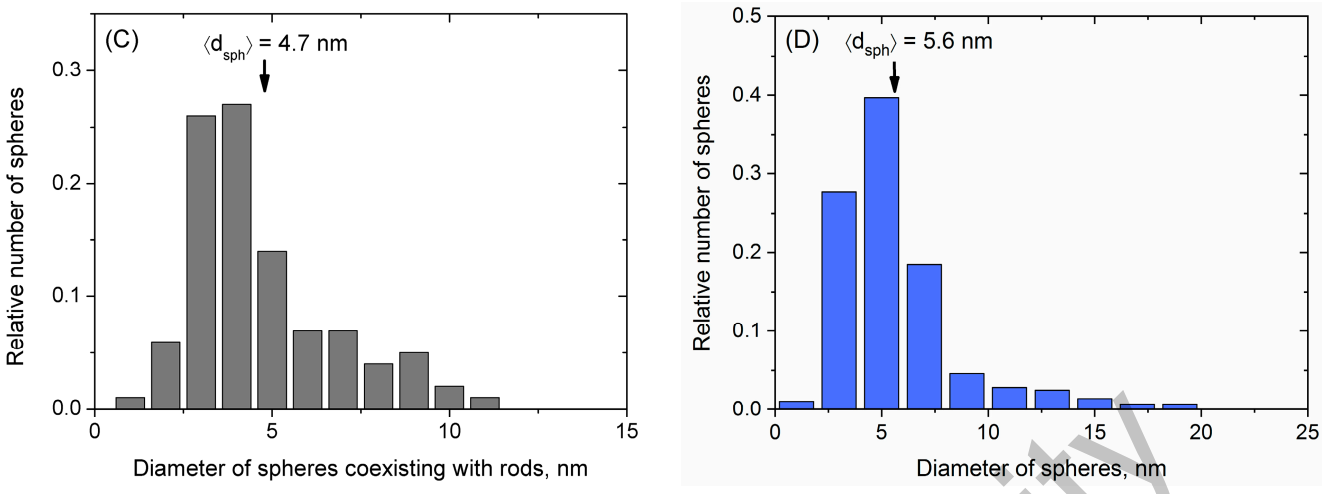

Figure 2. Size distribution histograms of NPs obtained from TEM micrographs: length (**A**) and diameter (**B**) of nanorods synthesized under magnetic field; diameter of spheres co-existing with nanorods (**C**); diameter of NPs synthesized in the absence of magnetic field (**D**). The numbers indicated in the diagrams are relative to the total number of particles analyzed (which was between 100 and 200).

The presence of a magnetic field is a principal factor in obtaining the nanorods. Indeed, under the same conditions but in the absence of a magnetic field, there are only isotropic spherical NPs (Figure 1B) with mean diameters of $<d_{sph}>$ = 5.6 nm (Figure 2D). This is consistent with the literature data, where the size of the prepared spherical NPs in the sub-10 nm range by the co-precipitation of Fe^{3+} and Co^{2+} was reported to be dependent on the reaction conditions, e.g., temperature [43,48].

The crystal structure of the synthesized NPs was investigated by TEM. It was shown that the nanorods obtained under a magnetic field are single crystalline (Figure 3A), and the {220} crystallographic planes of cobalt ferrite [49] with a characteristic plane spacing of 2.9 Å can be identified at the micrograph. Isotropic NPs co-existing with nanorods are also single crystals, and {311} planes with spacings of 2.5 Å [50] are seen (Figure 3B). The energy dispersive X-ray (EDX) spectrum shows that the ratio of Fe to Co atoms in the synthesized NPs is close to 2 (Figure 3C), which corresponds to that in the $CoFe_2O_4$ phase (C and Cu peaks at the EDX spectrum arise due to the substrate used in TEM measurements). Thus, HR TEM results show that the co-precipitation of Fe^{3+} and Co^{2+} ions in the magnetic field results in obtaining cobalt ferrite single nanocrystals. Note that NPs synthesized in the absence of a magnetic field are also single crystalline (Figure 3D).

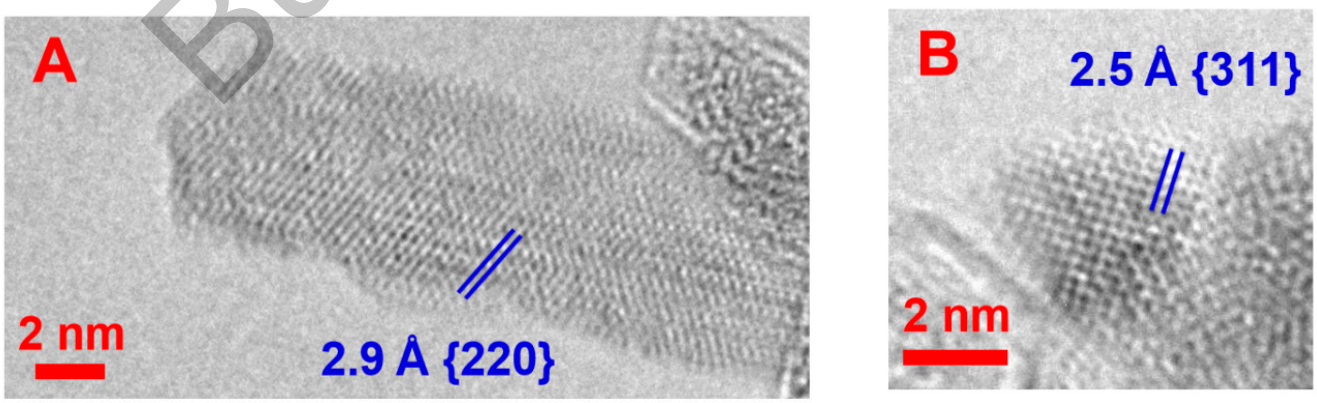

Figure 3. *Cont.*

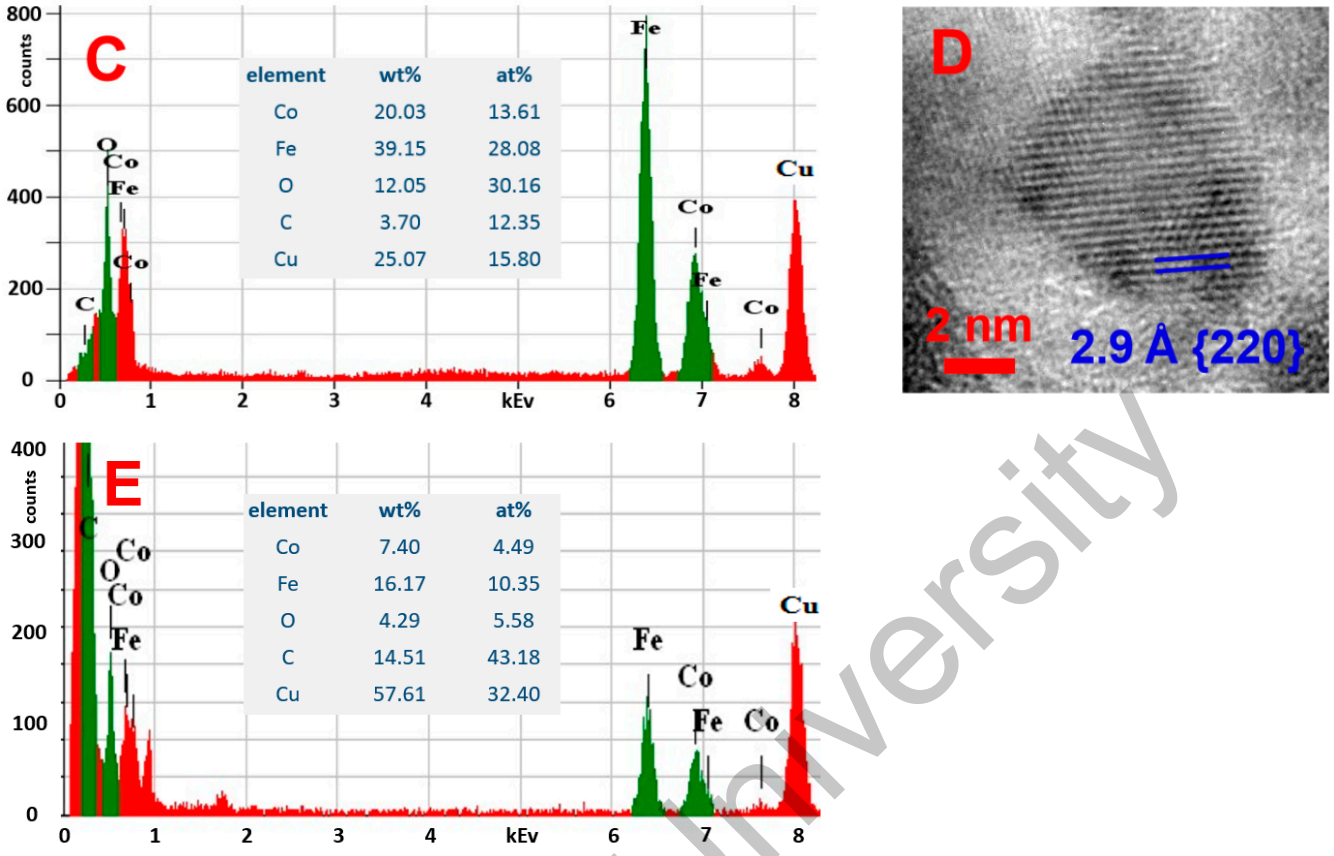

Figure 3. (**A**,**B**) HR TEM micrographs of NPs synthesized under a magnetic field of 0.4 T: (**A**)—nanorod; (**B**)—sphere; (**C**) energy-dispersive X-ray (EDX) spectrum for the sample synthesized under a magnetic field; (**D**) HR TEM micrograph of an NP synthesized in the absence of a magnetic field; (**E**) energy-dispersive X-ray (EDX) spectrum for the sample synthesized in the absence of a magnetic field. In the HR TEM pictures, crystallographic planes and plane spacing distances of cobalt ferrite are identified.

In order to identify the phase composition of the synthesized NPs, XRD (Figure 4) and Raman spectroscopy (Figure 5) were employed. The XRD pattern of the NPs synthesized in the magnetic field (Figure 4b) is consistent with a powder diffraction pattern of a $Co_{3-x}Fe_xO_4$ spinel structure (Figure 4c), which was calculated using Profex 5.2.7 software [51] based on a crystal structure from Ref. [52] with a lattice constant of a = 8.36 Å. This lattice constant confirms the composition with $x \approx 2$ (for pure $CoFe_2O_4$, a = 8.381 Å, for pure Co_2FeO_4, a = 8.242 Å) [52], proving the formation of the $CoFe_2O_4$ inverse spinel. Isotropic particles prepared without a magnetic field produce a much weaker pattern with broader lines (Figure 4a), which is due to the small size of NPs. However, the most intensive (311) spinel reflection at $2\theta \approx 35.5^\circ$ is also detected. A slight shift of the diffraction peak to lower angles is observed for the spheres (synthesized without magnetic field) compared to the rods (obtained in magnetic field). This may be due to a change in composition [52] or to structural strains in the samples [53]. We believe that the shifts of XRD peaks are due to the minor changes in the elemental composition of the crystals, which is confirmed by XPS data (presented below) showing that cobalt ferrite spheres have a slightly higher content of iron than nanorods (note that the EDX data in Figure 3 show the same trend—the atomic ratio Fe:Co is 2.06 for rods and 2.31 for spheres). A higher amount of iron increases the lattice constant, so XRD peaks shift to lower 2θ values.

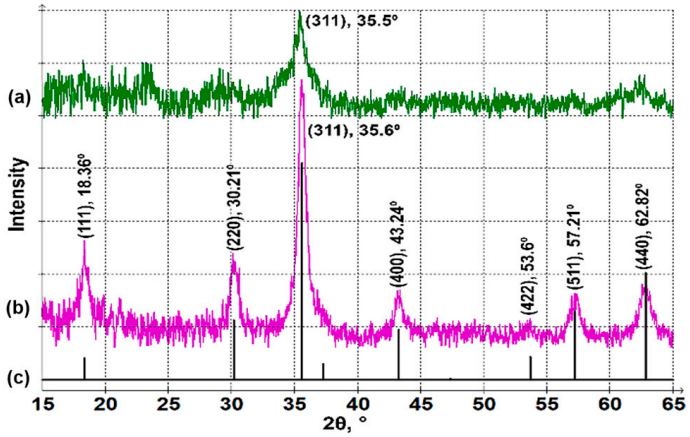

Figure 4. XRD patterns of $CoFe_2O_4$ NPs synthesized in the absence (**a**) and presence (**b**) of a magnetic field and calculated for $Co_{3-x}Fe_xO_4$ powder (**c**).

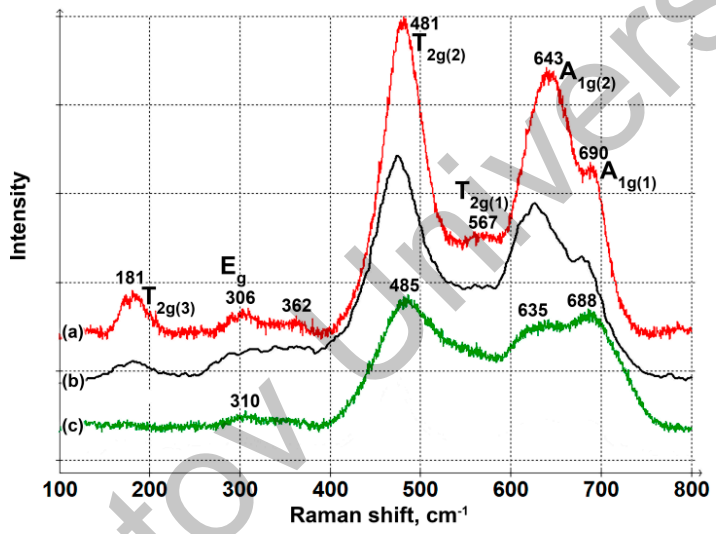

Figure 5. Raman spectra for cobalt ferrite NPs synthesized in the presence (**a**) and absence (**c**) of a magnetic field; Raman spectrum for $CoFe_2O_4$ nanoparticles [54] (**b**); Reproduced with permission from [54], ACS Publications, 2009.

The Raman spectrum of rod-like NPs (Figure 5a) is in perfect agreement with that reported for $CoFe_2O_4$ nanoparticles in the literature [54] (Figure 5b). The peaks at 643 and 690 cm^{-1} correspond to the highest frequency A1g mode split into two due to cation inversion [55,56]. These modes involve the symmetric stretching of an oxygen atom with respect to a metal ion in a tetrahedral void. The modes below 600 cm^{-1} involve symmetrical or asymmetrical bending of metal–oxygen bonding in octahedral sites. They have T2g (567, 481, and 181 cm^{-1}) or Eg (306 cm^{-1}) symmetries. The spectrum of NPs synthesized in the absence of a magnetic field has broader lines, which is due to the small NP size, but the main bands are visible and coincide with the $CoFe_2O_4$ structure. Therefore, XRD and Raman spectroscopy confirm that the NPs synthesized both in the presence and absence of a magnetic field have a spinel $CoFe_2O_4$ structure.

The high-resolution XPS spectra of NPs are presented in Figure 6. Overlapping with Co LMM and Fe LMM Auger lines complicates the analysis of the Fe 2p and, especially Co2p spectra. Both the Fe2p (Figure 6A) and Co2p (Figure 6B) spectra are virtually the same for the rods and spheres. The Fe2p spectra (Figure 6A) show a doublet of the $Fe2p_{3/2}$ and $Fe2p_{1/2}$ lines at binding energies of 711.1 and 724.6 eV with a series of shake-up satellites separated for about 8 and 18 eV from the main lines. Both the position and the satellite structure of the Fe2p spectra are typical for Fe^{3+} species in iron oxides [47,57]. The synthetic

component proposed for Fe^{3+} species in [58] fits the Fe2p spectra of NPs. The Co 2p XPS spectra of the samples demonstrate well-pronounced shake-up satellites shifted for about 6.5 eV to higher binding energies from the main $Co2p_{3/2}$ and $Co2p_{1/2}$ lines located at 780.5 and 796.3 eV. These spectra are typical for Co^{2+} species in cobalt oxides [59]. The O1s spectra (Figure 6C), along with the lattice oxygen peak at 530.1 eV, contain two additional peaks. The peak at 531.5 eV can be attributed to surface hydroxide and carbonate species, while the peak at 533.5 eV can be assigned to single O−C bonds in adventitious carbon on the surface. Such oxygen spectra are typical for the ex situ prepared metal oxide samples. Summarizing, the XPS data confirm that both samples mainly contain Fe^{3+} and Co^{2+} species coordinated with lattice oxygen.

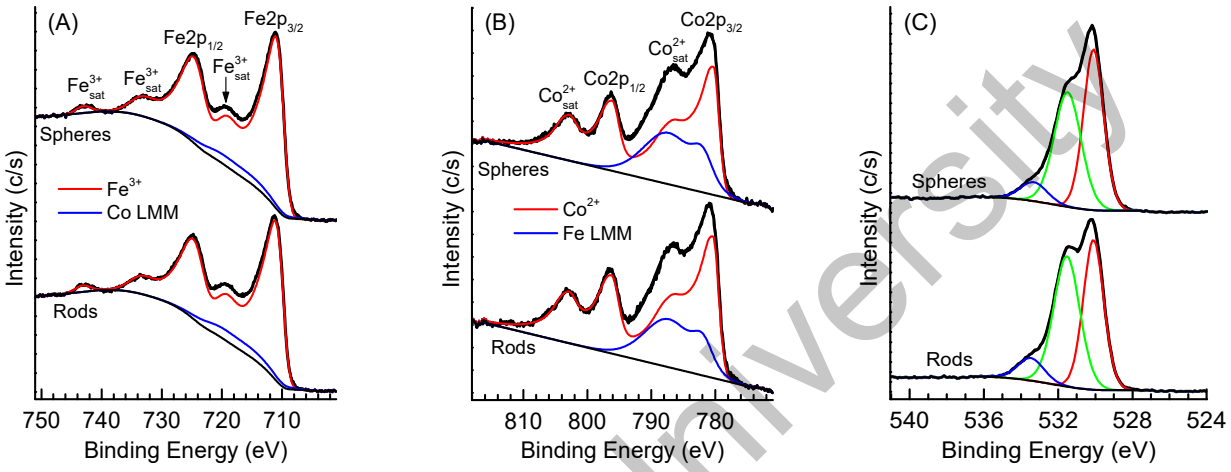

Figure 6. High-resolution Fe2p (**A**), Co2p (**B**), and O1s (**C**) XPS spectra of NPs.

These results suggest a mechanism for the anisotropic growth of rod-like cobalt ferrite NPs in the magnetic field (Figure 7), which is similar to the mechanism proposed earlier for the magnetic-field-assisted synthesis of rod-like magnetite [32]. At the first stage of the co-precipitation reaction, small isotropic "seed" NPs are formed. At this stage, most of the OH^- ions of alkali are consumed for the formation of cobalt ferrite according to the following reaction:

$$Co^{2+} + 2Fe^{3+} + 8\,OH^- \rightarrow CoFe_2O_4 + 4H_2O \quad (1)$$

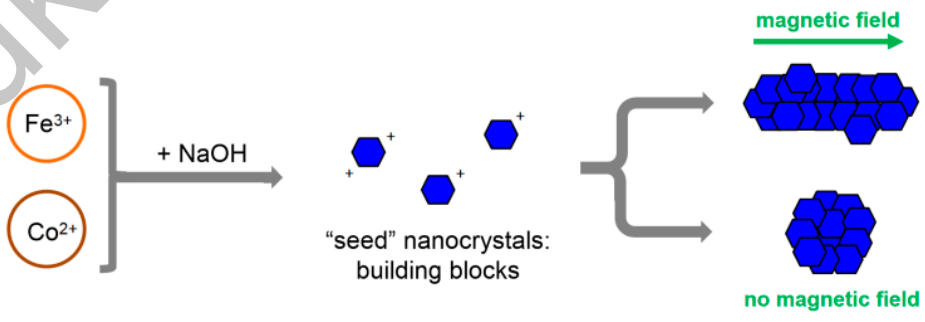

Figure 7. Schematic representation of the growth mechanism of cobalt ferrite nanorods in the presence and absence of a magnetic field.

This induces a drop in pH from an initial value of ~14 to ~6.3, which was measured for the syntheses carried out in the present work. $CoFe_2O_4$ has an isoelectric point of ca. 7 [60]; therefore, at pH 6.3, the "seed" NPs are only slightly positively charged. Thus, electrostatic repulsion between the "seeds" is not strong enough to prevent self-assembly into columnar structures due to magnetization obtained in the external magnetic field [61]. At the latter reaction stages, the "seeds", which are assembled together, fuse into a single-crystalline

rod. The growth of rods by aggregation and the re-crystallization of primary particles in the magnetic field was previously described for micrometer-sized rod-like magnetite particles synthesized by co-precipitation [28]. This resembles the general features of the nanoparticles' growth [62]. In the absence of a magnetic field, the "seeds" do not fuse into rods but into some larger isotropic NPs (Figure 7).

The magnetic properties of synthesized cobalt ferrite NPs were studied with magnetometry. In Figure 8a, the hysteresis curves, obtained from the VSM measurements at room temperature (300 K), are depicted. The values of saturation magnetization M_s and coercivity H_c determined from the curves (Figure 8b) are presented in Table 1. In Figure 8a, one can see that the size of the hysteresis loop is much larger for nanorods. As a consequence, the sample containing nanorods demonstrates significantly higher values of M_s and H_c (Figure 8b), which indicates that nanorods possess stronger magnetic properties than isotropic NPs. The rise of saturation magnetization and coercivity with the size of monocrystalline $CoFe_2O_4$ NPs was previously described in the literature [63]. It was explained by increasing the size of magnetic domains where the atomic spins are aligned along the direction of the applied magnetic field. As a result, the maximum magnetization of the particles and the strength of the reverse external field required to demagnetize them increased [63].

Obtained nanoparticles are single crystals (Figure 3A), and they have slightly lower but comparable magnetic properties compared to larger polycrystalline particles [35] and bulk $CoFe_2O_4$ [64]. An increase in the nanocrystal size induces a rise of saturation magnetization, reaching 80 emu/g for 50 nm NPs and not increasing further up to the bulk. The coercive force shows a non-linear dependence on the NP size. A maximum of 1.2 kOe is reached for 25 nm NPs, and it is lower for both smaller (as in this work, where it equals 0.6 kOe) and larger NPs. For the bulk, the coercive force is only 0.06 kOe.

Table 1. Values of saturation magnetization M_s and coercivity H_c anisotropic cobalt ferrite nanorods before and after 1 h of aging at 80 °C in comparison with isotropic cobalt ferrite NPs.

	M_s, emu/g	H_c, Oe
Isotropic $CoFe_2O_4$ NPs	0.3	111
$CoFe_2O_4$ nanorods	8.3	248
$CoFe_2O_4$ nanorods after 1 h of aging	28.5	265

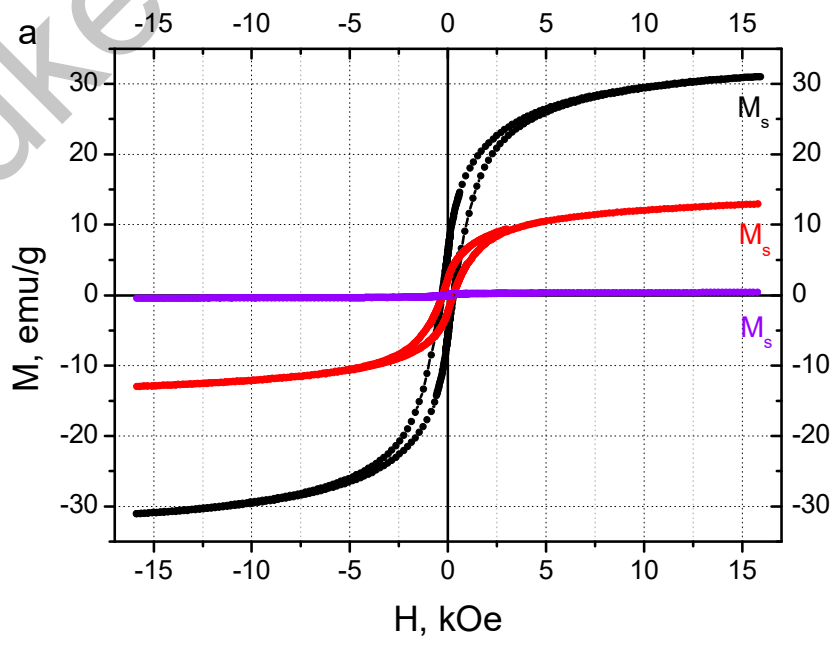

Figure 8. *Cont.*

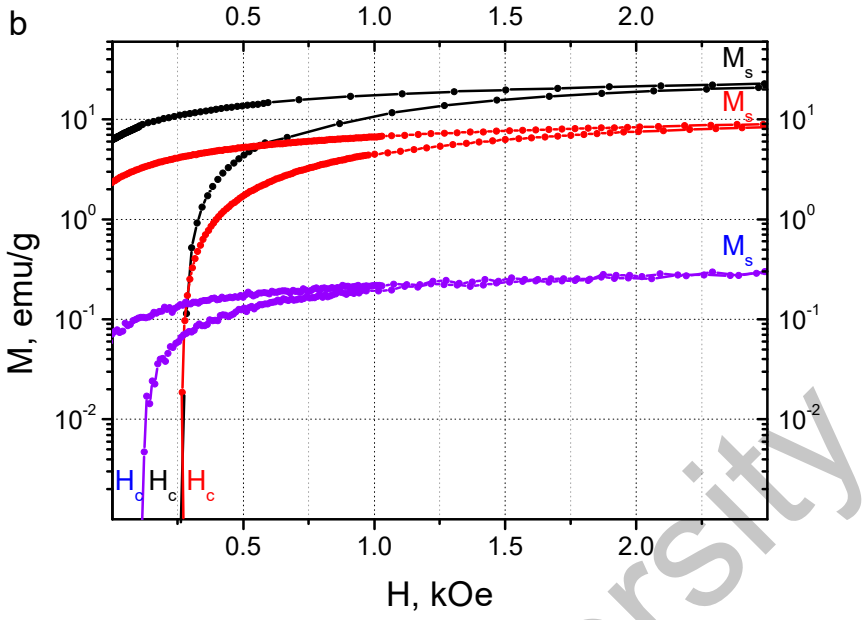

Figure 8. Magnetic hysteresis loops of isotropic cobalt ferrite NPs (violet) and anisotropic cobalt ferrite nanorods before (red) and after (black) aging for 1 h at 80 °C (**a**); the enlargement of the loops at low strength of the applied magnetic field (**b**).

The solution of synthesized nanorods was aged at 80 °C to increase the magnetic properties [65]. The hysteresis loop of the nanorods after aging for 1 h demonstrates a 3 times higher value of saturation magnetization M_s, than nanorods before aging (Figure 8a, Table 1). The increase in M_s upon aging can be attributed to the increased size of the crystallite, as was suggested by F. Huixia and co-authors [65] for aged isotropic $CoFe_2O_4$ NPs. Unlike M_s, the value of coercivity H_c of the nanorods before and after aging remains almost the same (Table 1). Probably, the temperature of aging is not high enough to additionally adjust the aligned atomic spins inside the rod-like particles. Longer aging up to 250 h (Figure 9) does not affect the M_s and H_c values (see Supplementary Information for the corresponding hysteresis loops). Therefore, 1 h of aging is enough to obtain anisotropic $CoFe_2O_4$ NPs with maximum saturation magnetization M_s and coercivity H_c, which are equal to 30 ± 1 emu/g and 330 ± 15 Oe, respectively.

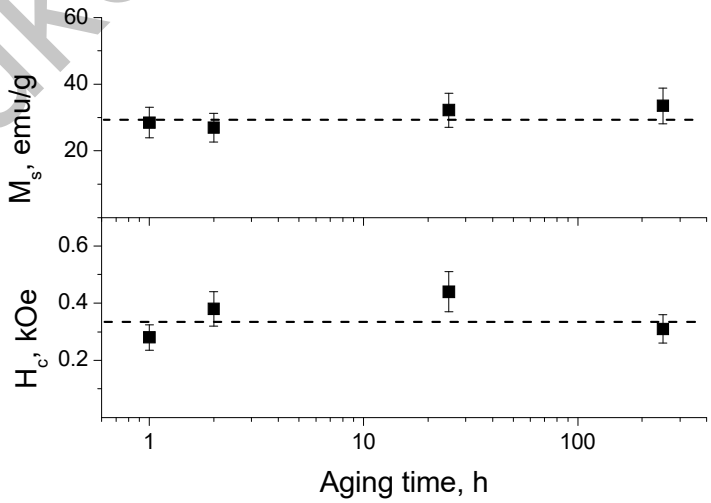

Figure 9. Dependences of saturation magnetization M_s and coercivity H_c of cobalt ferrite nanorods on aging time at 80 °C.

4. Conclusions

In this paper, it is shown, for the first time, that a static magnetic field of moderate strength can be used as a template for the anisotropic growth of cobalt ferrite NPs, which is one of the most attractive nanomaterials in many applications. Nanorods with an aspect ratio of ca. 7 are synthesized by the co-precipitation of Fe^{3+} and Co^{2+} ions in alkali. They are single crystals and co-exist with some spherical NPs. EDX, XRD, and Raman spectroscopy confirm the formation of a $CoFe_2O_4$ spinel structure. The magnetic field is demonstrated to be a key factor that provides anisotropic growth at the same synthesis conditions. But, in the absence of a magnetic field, only small isotropic $CoFe_2O_4$ NPs are obtained. It was suggested that anisotropic cobalt ferrite NP growth proceeds in two steps: (1) the formation of "seed" NPs and (2) the self-assembly of "seeds" into columns in the magnetic field and their fusion into single-crystal nanorods. According to VSM data, the maximum values of saturation magnetization Ms and coercivity Hc of the nanorods are obtained after 1 h of aging at 80 °C and equaled 30 emu/g and 0.33 kOe, respectively. The results of this paper demonstrate that a facile and "green" magnetic-field-assisted synthesis of anisotropic NPs with pronounced magnetic properties can be applied not only to magnetite but also other metal oxides. This opens a route for simplifying the production of anisotropic magnetic nanoparticles, which are currently synthesized mostly by rather complex methods. The surface of the obtained nanorods is free of additional stabilizers and can be further easily modified. Cobalt ferrite nanorods may be used in various practical applications, including biomedicine, energy storage, green energy production, and the preparation of magnetic nanocomposites and gels with controlled anisotropy.

Supplementary Materials: The following supporting information can be downloaded at https://www.mdpi.com/article/10.3390/nano14060541/s1, Figure S1: hysteresis loops of cobalt ferrite nanorods after aging for different periods of time at 80 °C.

Author Contributions: Conceptualization, O.E.P., A.V.S. and A.L.K.; methodology, O.E.P., A.V.S. and A.L.K.; investigation, D.E.K., I.S.T., E.D.S., K.I.M. and P.V.S.; writing—original draft preparation, A.V.S., K.I.M. and A.L.K.; writing—review and editing, I.A.K., D.A.M., O.E.P. and A.V.S.; funding acquisition, A.V.S. and A.L.K. All authors have read and agreed to the published version of the manuscript.

Funding: This work was financially supported by the Russian Science Foundation, project № 21-73-10197.

Data Availability Statement: The data presented in this study are openly available.

Acknowledgments: The authors acknowledge support from the Lomonosov Moscow State University Program of Development for providing access to the XPS facility.

Conflicts of Interest: The authors declare no conflicts of interest.

References

1. Laurent, S.; Forge, D.; Port, M.; Roch, A.; Robic, C.; Vander Elst, L.; Muller, R.N. Magnetic Iron Oxide Nanoparticles: Synthesis, Stabilization, Vectorization, Physicochemical Characterizations, and Biological Applications. *Chem. Rev.* **2008**, *108*, 2064–2110. [CrossRef] [PubMed]
2. Baumgartner, J.; Dey, A.; Bomans, P.H.H.; Le Coadou, C.; Fratzl, P.; Sommerdijk, N.A.J.M.; Faivre, D. Nucleation and Growth of Magnetite from Solution. *Nat. Mater.* **2013**, *12*, 310–314. [CrossRef] [PubMed]
3. Zhu, K.; Ju, Y.; Xu, J.; Yang, Z.; Gao, S.; Hou, Y. Magnetic Nanomaterials: Chemical Design, Synthesis, and Potential Applications. *Acc. Chem. Res.* **2018**, *51*, 404–413. [CrossRef] [PubMed]
4. Cerdan, K.; Moya, C.; Van Puyvelde, P.; Bruylants, G.; Brancart, J. Magnetic Self-Healing Composites: Synthesis and Applications. *Molecules* **2022**, *27*, 3796. [CrossRef]
5. Shibaev, A.; Smirnova, M.; Kessel, D.; Bedin, S.; Razumovskaya, I.; Philippova, O. Remotely Self-Healable, Shapeable and pH-Sensitive Dual Cross-Linked Polysaccharide Hydrogels with Fast Response to Magnetic Field. *Nanomaterials* **2021**, *11*, 1271. [CrossRef]
6. Kim, Y.; Zhao, X. Magnetic Soft Materials and Robots. *Chem. Rev.* **2022**, *122*, 5317–5364. [CrossRef]
7. Zhu, T.; Chen, J.S.; Lou, X.W. Glucose-Assisted One-Pot Synthesis of FeOOH Nanorods and Their Transformation to Fe_3O_4@Carbon Nanorods for Application in Lithium Ion Batteries. *J. Phys. Chem. C* **2011**, *115*, 9814–9820. [CrossRef]

8. Guan, D.; Wang, B.; Zhang, J.; Shi, R.; Jiao, K.; Li, L.; Wang, Y.; Xie, B.; Zhang, Q.; Yu, J.; et al. Hydrogen society: From present to future. *Energy Environ. Sci.* **2023**, *16*, 4926. [CrossRef]
9. Pardo, A.; Gómez-Florit, M.; Barbosa, S.; Taboada, P.; Domingues, R.M.A.; Gomes, M.E. Magnetic Nanocomposite Hydrogels for Tissue Engineering: Design Concepts and Remote Actuation Strategies to Control Cell Fate. *ACS Nano* **2021**, *15*, 175–209. [CrossRef]
10. Veloso, S.R.S.; Andrade, R.G.D.; Castanheira, E.M.S. Review on the Advancements of Magnetic Gels: Towards Multifunctional Magnetic Liposome-Hydrogel Composites for Biomedical Applications. *Adv. Colloid Interface Sci.* **2021**, *288*, 102351. [CrossRef]
11. Silva, M.P.; Drummond, A.L.; Aquino, V.R.R.; Silva, L.P.; Azevedo, R.B.; Sales, M.J.A.; Morais, P.C.; Bakuzis, A.F.; Sousa, M.H. Facile Green Synthesis of Nanomagnets for Modulating Magnetohyperthermia: Tailoring Size, Shape and Phase. *RSC Adv.* **2017**, *7*, 47669–47680. [CrossRef]
12. Mohapatra, J.; Mitra, A.; Tyagi, H.; Bahadur, D.; Aslam, M. Iron Oxide Nanorods as High-Performance Magnetic Resonance Imaging Contrast Agents. *Nanoscale* **2015**, *7*, 9174–9184. [CrossRef]
13. Shibaev, A.V.; Osiptsov, A.A.; Philippova, O.E. Novel Trends in the Development of Surfactant-Based Hydraulic Fracturing Fluids: A Review. *Gels* **2021**, *7*, 258. [CrossRef]
14. Pearce, A.K.; Wilks, T.R.; Arno, M.C.; O'Reilly, R.K. Synthesis and Applications of Anisotropic Nanoparticles with Precisely Defined Dimensions. *Nat. Rev. Chem.* **2020**, *5*, 21–45. [CrossRef]
15. Lisjak, D.; Mertelj, A. Anisotropic Magnetic Nanoparticles: A Review of Their Properties, Syntheses and Potential Applications. *Prog. Mater. Sci.* **2018**, *95*, 286–328. [CrossRef]
16. Andrade, R.G.D.; Veloso, S.R.S.; Castanheira, E.M.S. Shape Anisotropic Iron Oxide-Based Magnetic Nanoparticles: Synthesis and Biomedical Applications. *Int. J. Mol. Sci.* **2020**, *21*, 2455. [CrossRef]
17. Orza, A.; Wu, H.; Xu, Y.; Lu, Q.; Mao, H. One-Step Facile Synthesis of Highly Magnetic and Surface Functionalized Iron Oxide Nanorods for Biomarker-Targeted Applications. *ACS Appl. Mater. Interfaces* **2017**, *9*, 20719–20727. [CrossRef] [PubMed]
18. Sun, H.; Chen, B.; Jiao, X.; Jiang, Z.; Qin, Z.; Chen, D. Solvothermal Synthesis of Tunable Electroactive Magnetite Nanorods by Controlling the Side Reaction. *J. Phys. Chem. C* **2012**, *116*, 5476–5481. [CrossRef]
19. Almeida, T.P.; Fay, M.W.; Zhu, Y.; Brown, P.D. Hydrothermal Growth Mechanism of α-Fe_2O_3 Nanorods Derived by near in Situ Analysis. *Nanoscale* **2010**, *2*, 2390. [CrossRef] [PubMed]
20. Woo, K.; Lee, H.J.; Ahn, J.-P.; Park, Y.S. Sol–Gel Mediated Synthesis of Fe_2O_3 Nanorods. *Adv. Mater.* **2003**, *15*, 1761–1764. [CrossRef]
21. Ahn, T.; Kim, J.H.; Yang, H.-M.; Lee, J.W.; Kim, J.-D. Formation Pathways of Magnetite Nanoparticles by Coprecipitation Method. *J. Phys. Chem. C* **2012**, *116*, 6069–6076. [CrossRef]
22. Kumar, R.V.; Koltypin, Y.; Xu, X.N.; Yeshurun, Y.; Gedanken, A.; Felner, I. Fabrication of Magnetite Nanorods by Ultrasound Irradiation. *J. Appl. Phys.* **2001**, *89*, 6324–6328. [CrossRef]
23. Feng, L.; Jiang, L.; Mai, Z.; Zhu, D. Polymer-Controlled Synthesis of Fe_3O_4 Single-Crystal Nanorods. *J. Colloid Interface Sci.* **2004**, *278*, 372–375. [CrossRef] [PubMed]
24. Zhou, Z.; Zhu, X.; Wu, D.; Chen, Q.; Huang, D.; Sun, C.; Xin, J.; Ni, K.; Gao, J. Anisotropic Shaped Iron Oxide Nanostructures: Controlled Synthesis and Proton Relaxation Shortening Effects. *Chem. Mater.* **2015**, *27*, 3505–3515. [CrossRef]
25. Chhatre, A.; Duttagupta, S.; Thaokar, R.; Mehra, A. Mechanism of Nanorod Formation by Wormlike Micelle-Assisted Assembly of Nanospheres. *Langmuir* **2015**, *31*, 10524–10531. [CrossRef]
26. Yougbaré, S.; Mutalik, C.; Chung, P.-F.; Krisnawati, D.I.; Rinawati, F.; Irawan, H.; Kristanto, H.; Kuo, T.-R. Gold Nanorod-Decorated Metallic MoS_2 Nanosheets for Synergistic Photothermal and Photodynamic Antibacterial Therapy. *Nanomaterials* **2021**, *11*, 3064. [CrossRef] [PubMed]
27. Wu, M.; Xiong, Y.; Jia, Y.; Niu, H.; Qi, H.; Ye, J.; Chen, Q. Magnetic Field-Assisted Hydrothermal Growth of Chain-like Nanostructure of Magnetite. *Chem. Phys. Lett.* **2005**, *401*, 374–379. [CrossRef]
28. Vereda, F.; De Vicente, J.; Hidalgo-Álvarez, R. Influence of a Magnetic Field on the Formation of Magnetite Particles via Two Precipitation Methods. *Langmuir* **2007**, *23*, 3581–3589. [CrossRef]
29. Zhang, C.; Mo, Z.; Guo, R.; Teng, G.; Zhao, G. Magnetic-Field-Induced Synthesis of Fe_3O_4 Nanorods by a Gas–Liquid Interfacial Process: Microstructure Control, Magnetic and Photocatalytic Properties. *Mater. Res. Bull.* **2014**, *53*, 116–122. [CrossRef]
30. Zhang, W.; Jia, S.; Wu, Q.; Ran, J.; Wu, S.; Liu, Y. Convenient Synthesis of Anisotropic Fe_3O_4 Nanorods by Reverse Co-Precipitation Method with Magnetic Field-Assisted. *Mater. Lett.* **2011**, *65*, 1973–1975. [CrossRef]
31. Yang, X.; Yu, P.; Moats, M.S.; Zhang, X. Wet Chemical Synthesis of High Aspect Ratio Magnetite Rods. *Powder Technol.* **2011**, *212*, 439–444. [CrossRef]
32. Shibaev, A.V.; Shvets, P.V.; Kessel, D.E.; Kamyshinsky, R.A.; Orekhov, A.S.; Abramchuk, S.S.; Khokhlov, A.R.; Philippova, O.E. Magnetic-Field-Assisted Synthesis of Anisotropic Iron Oxide Particles: Effect of pH. *Beilstein J. Nanotechnol.* **2020**, *11*, 1230–1241. [CrossRef] [PubMed]
33. Hu, L.; Zhang, R.; Chen, Q. Synthesis and Assembly of Nanomaterials under Magnetic Fields. *Nanoscale* **2014**, *6*, 14064–14105. [CrossRef]
34. Rani, B.J.; Ravina, M.; Saravanakumar, B.; Ravi, G.; Ganesh, V.; Ravichandran, S.; Yuvakkumar, R. Ferrimagnetism in Cobalt Ferrite ($CoFe_2O_4$) Nanoparticles. *Nano-Struct. Nano-Objects* **2018**, *14*, 84–91. [CrossRef]

35. Maaz, K.; Mumtaz, A.; Hasanain, S.K.; Ceylan, A. Synthesis and Magnetic Properties of Cobalt Ferrite ($CoFe_2O_4$) Nanoparticles Prepared by Wet Chemical Route. *J. Magn. Magn. Mater.* **2007**, *308*, 289–295. [CrossRef]
36. Farahmandjou, M.; Honarbakhsh, S.; Behrouzinia, S. PVP-Assisted Synthesis of Cobalt Ferrite ($CoFe_2O_4$) Nanorods. *Phys. Chem. Res.* **2016**, *4*, 655–662. [CrossRef]
37. Antonel, P.S.; Oliveira, C.L.P.; Jorge, G.A.; Perez, O.E.; Leyva, A.G.; Negri, R.M. Synthesis and Characterization of $CoFe_2O_4$ Magnetic Nanotubes, Nanorods and Nanowires. Formation of Magnetic Structured Elastomers by Magnetic Field-Induced Alignment of $CoFe_2O_4$ Nanorods. *J. Nanopart. Res.* **2015**, *17*, 294. [CrossRef]
38. Ji, G.B.; Tang, S.L.; Ren, S.K.; Zhang, F.M.; Gu, B.X.; Du, Y.W. Simplified Synthesis of Single-Crystalline Magnetic $CoFe_2O_4$ Nanorods by a Surfactant-Assisted Hydrothermal Process. *J. Cryst. Growth* **2004**, *270*, 156–161. [CrossRef]
39. Sodaee, T.; Ghasemi, A.; Razavi, R.S. Controlled Growth of Large-Area Arrays of Gadolinium-Substituted Cobalt Ferrite Nanorods by Hydrothermal Processing without Use of Any Template. *Ceram. Int.* **2016**, *42*, 17420–17428. [CrossRef]
40. Wu, X.; Wang, W.; Song, N.; Yang, X.; Khaimanov, S.; Tsidaeva, N. From Nanosphere to Nanorod: Tuning Morphology, Structure and Performance of Cobalt Ferrites via Pr^{3+} Doping. *Chem. Eng. J.* **2016**, *306*, 382–392. [CrossRef]
41. Jia, Z.; Ren, D.; Zhu, R. Synthesis, Characterization and Magnetic Properties of $CoFe_2O_4$ Nanorods. *Mater. Lett.* **2012**, *66*, 128–131. [CrossRef]
42. Zhang, X.; Kan, X.; Wang, M.; Rao, R.; Zheng, G.; Wang, M.; Ma, Y. The Magnetic Property of $CoFe_2O_4$ Assembly by the Gradient Magnetic Field. *J. Cryst. Growth* **2021**, *565*, 126131. [CrossRef]
43. Stein, C.R.; Bezerra, M.T.S.; Holanda, G.H.A.; André-Filho, J.; Morais, P.C. Structural and Magnetic Properties of Cobalt Ferrite Nanoparticles Synthesized by Co-Precipitation at Increasing Temperatures. *AIP Adv.* **2018**, *8*, 056303. [CrossRef]
44. Gervits, L.L.; Shibaev, A.V.; Gulyaev, M.V.; Molchanov, V.S.; Anisimov, N.V.; Pirogov, Y.A.; Khokhlov, A.R.; Philippova, O.E. A Facile Method of Preparation of Polymer-Stabilized Perfluorocarbon Nanoparticles with Enhanced Contrast for Molecular Magnetic Resonance Imaging. *BioNanoScience* **2017**, *7*, 456–463. [CrossRef]
45. Schneider, C.A.; Rasband, W.S.; Eliceiri, K.W. NIH Image to ImageJ: 25 Years of Image Analysis. *Nat. Methods* **2012**, *9*, 671–675. [CrossRef] [PubMed]
46. Shvets, P.; Dikaya, O.; Maksimova, K.; Goikhman, A. A Review of Raman Spectroscopy of Vanadium Oxides. *J. Raman Spectrosc.* **2019**, *50*, 1226–1244. [CrossRef]
47. Gota, S.; Guiot, E.; Henriot, M.; Gautier-Soyer, M. Atomic-oxygen-assisted MBE growth of $\alpha-Fe_2O_3$ on $\alpha-Al_2O_3(0001)$: Metastable FeO(111)-like phase at subnanometer thicknesses. *Phys. Rev. B* **1999**, *60*, 14387–14395. [CrossRef]
48. Kim, Y.I.; Kim, D.; Lee, C.S. Synthesis and Characterization of $CoFe_2O_4$ Magnetic Nanoparticles Prepared by Temperature-Controlled Coprecipitation Method. *Phys. B Condens. Matter* **2003**, *337*, 42–51. [CrossRef]
49. Mitra, S.; Veluri, P.S.; Chakraborthy, A.; Petla, R.K. Electrochemical Properties of Spinel Cobalt Ferrite Nanoparticles with Sodium Alginate as Interactive Binder. *ChemElectroChem* **2014**, *1*, 1068–1074. [CrossRef]
50. Kalam, A.; Al-Sehemi, A.G.; Assiri, M.; Du, G.; Ahmad, T.; Ahmad, I.; Pannipara, M. Modified Solvothermal Synthesis of Cobalt Ferrite ($CoFe_2O_4$) Magnetic Nanoparticles Photocatalysts for Degradation of Methylene Blue with H_2O_2/Visible Light. *Results Phys.* **2018**, *8*, 1046–1053. [CrossRef]
51. Doebelin, N.; Kleeberg, R. Profex: A Graphical User Interface for the Rietveld Refinement Program BGMN. *J. Appl. Crystallogr.* **2015**, *48*, 1573–1580. [CrossRef]
52. Ferreira, T.A.S.; Waerenborgh, J.C.; Mendonça, M.H.R.M.; Nunes, M.R.; Costa, F.M. Structural and Morphological Characterization of $FeCo_2O_4$ and $CoFe_2O_4$ Spinels Prepared by a Coprecipitation Method. *Solid State Sci.* **2003**, *5*, 383–392. [CrossRef]
53. Guan, D.; Shi, C.; Xu, H.; Gu, Y.; Zhong, J.; Sha, Y.; Hu, Z.; Ni, M.; Shao, Z. Simultaneously mastering operando strain and reconstruction effects via phase-segregation strategy for enhanced oxygen-evolving electrocatalysis. *J. Energy Chem.* **2023**, *82*, 572–580. [CrossRef]
54. Jacintho, G.V.M.; Brolo, A.G.; Corio, P.; Suarez, P.A.Z.; Rubim, J.C. Structural Investigation of MFe_2O_4 (M = Fe, Co) Magnetic Fluids. *J. Phys. Chem. C* **2009**, *113*, 7684–7691. [CrossRef]
55. Chandramohan, P.; Srinivasan, M.P.; Velmurugan, S.; Narasimhan, S.V. Cation Distribution and Particle Size Effect on Raman Spectrum of $CoFe_2O_4$. *J. Solid State Chem.* **2011**, *184*, 89–96. [CrossRef]
56. Kumari, M.; Bhatnagar, M.C. Study of Structural and Magnetic Properties of Cobalt Ferrite Nanoparticles Sintered at Different Temperature. *AIP Conf. Proc.* **2018**, *1953*, 120075. [CrossRef]
57. Bagus, P.S.; Nelin, C.J.; Brundle, C.R.; Crist, B.V.; Lahiri, N.; Rosso, K.M. Combined multiplet theory and experiment for the Fe 2p and 3p XPS of FeO and Fe_2O_3. *J. Chem. Phys.* **2021**, *154*, 094709. [CrossRef] [PubMed]
58. Lokteva, E.S.; Shishova, V.V.; Maslakov, K.I.; Golubina, E.V.; Kharlanov, A.N.; Rodin, I.A.; Vokuev, M.F.; Filimonov, D.S.; Tolkachev, N.N. Bimetallic PdFe catalysts in hydrodechlorination of diclofenac: Influence of support nature, metal deposition sequence and reduction condition. *Appl. Surf. Sci.* **2023**, *613*, 156022. [CrossRef]
59. Qiao, L.; Xiao, H.Y.; Meyer, H.M.; Sun, J.N.; Rouleau, C.M.; Puretzky, A.A.; Geohegan, D.B.; Ivanov, I.N.; Yoon, M.; Weber, W.J.; et al. Nature of the band gap and origin of the electro-/photo-activity of Co_3O_4. *J. Mater. Chem. C* **2013**, *1*, 4628. [CrossRef]
60. Sanpo, N.; Tharajak, J.; Li, Y.; Berndt, C.C.; Wen, C.; Wang, J. Biocompatibility of Transition Metal-Substituted Cobalt Ferrite Nanoparticles. *J. Nanopart. Res.* **2014**, *16*, 2510. [CrossRef]

61. Zhang, Y.; Sun, L.; Fu, Y.; Huang, Z.C.; Bai, X.J.; Zhai, Y.; Du, J.; Zhai, H.R. The Shape Anisotropy in the Magnetic Field-Assisted Self-Assembly Chain-like Structure of Magnetite. *J. Phys. Chem. C* **2009**, *113*, 8152–8157. [CrossRef]
62. Luo, B.; Wang, Z.; Curk, T.; Watson, G.; Liu, C.; Kim, A.; Ou, Z.; Luijten, E.; Chen, Q. Unravelling Crystal Growth of Nanoparticles. *Nat. Nanotechnol.* **2023**, *18*, 589–595. [CrossRef] [PubMed]
63. Kumar, V.; Rana, A.; Yadav, M.S.; Pant, R.P. Size-Induced Effect on Nano-Crystalline $CoFe_2O_4$. *J. Magn. Magn. Mater.* **2008**, *320*, 1729–1734. [CrossRef]
64. Nlebedim, I.C.; Snyder, J.E.; Moses, A.J.; Jiles, D.C. Effect of deviation from stoichiometric composition on structural and magnetic properties of cobalt ferrite, $Co_xFe_{3-x}O_4$ (x = 0.2 to 1.0). *J. Appl. Phys.* **2012**, *111*, 07D704. [CrossRef]
65. Huixia, F.; Baiyi, C.; Deyi, Z.; Jianqiang, Z.; Lin, T. Preparation and Characterization of the Cobalt Ferrite Nano-Particles by Reverse Coprecipitation. *J. Magn. Magn. Mater.* **2014**, *356*, 68–72. [CrossRef]